Curvature of n-Dimensional Space Curves in Grey-Value Images

Bernd Rieger and Lucas J. van Vliet

***Abstract*—Local curvature represents an important shape parameter of space curves which are well described by differential geometry. We have developed an estimator for local curvature of space curves embedded in n-dimensional (n-D) grey-value images. There is neither a segmentation of the curve needed nor a parametric model assumed. Our estimator works on the orientation field of the space curve. This orientation field and a description of local structure is obtained by the gradient structure tensor. The orientation field has discontinuities; walking around a closed contour yields two such discontinuities in orientation. This field is mapped via the Knutsson mapping to a continuous representation; from a n-D vector to a symmetric n^2-D tensor field. The curvature of a space curve, a coordinate invariant property, is computed in this tensor field representation. An extensive evaluation shows that our curvature estimation is unbiased even in the presence of noise, independent of the scale of the object and furthermore the relative error stays small.**

***Index Terms*—Curvature, gradient structure tensor, Knutsson mapping, space curves in n-D.**

I. Introduction

In this paper, we present a method suitable for curvature estimation of space curves, implicitly represented by grey-level isophotes (level-sets), in n-dimensional (n-D) images. The curve is embedded in the image by a grey-level difference with respect to the background. Our method works directly on the grey-value information of the image; neither a segmentation is needed to detect the curve nor a parametric fit is done at any time during the analysis. The method exploits the differential structure of images.

Curvature in two-dimensional (2-D) images has been well-studied, both in segmented and in grey-level images [1]–[5]. Curvature is the first-order shape descriptor of an object and, therefore, an important feature. In 2-D, it totally determines the shape of a curve.

Isophote curvature [6]–[8] can successfully be applied to edges in 2-D and three-dimensional (3-D) grey-value images, but it fails when applied to lines (space curves) [9]. To overcome the problems associated with isophote curvature, one transforms the grey-value image into an orientation map from which the curvature can be derived after solving the discontinuity problem [1]. In 2-D, the use of the double angle method is well-known [1], [10], but in 3-D it remained an obstacle that prevented the computation of curvature in 3-D. Therefore, traditional 3-D methods are applied to segmented images, or even on curves represented by ordered points, which enables one to fit a parametric model to the curve [11]–[14]. These methods rely heavily on the preceding segmentation, labeling, and orderings steps, which may fail due to noise or the presence of a bundle of space curves comparable to a lock of hair.

Manuscript received July 24, 2001; revised March 21, 2002. This work was supported in part by the Netherlands Organization for Scientific Research under Grant 612-012-003. The associate editor coordinating the review of this manuscript and approving it for publication was Prof. Ioannis Pitas.

The authors are with the Pattern Recognition Group, Department of Applied Physics, Delft University of Technology, 2628 Delft, The Netherlands (e-mail: bernd@ph.tn.tudelft.nl; lucas@ph.tn.tudelft.nl).

Publisher Item Identifier 10.1109/TIP.2002.800885.

A. Mathematics

First we present the mathematics of differential geometry that describe space curves. We have adopted a formulation that can be applied to grey-value images (Section II).

In 2-D, the curvature of a curve in every point describes the shape of this curve completely. In 3-D, a second parameter, the torsion, is needed to give a full description, in 4-D another, and so forth. For a n-dimensional curve, we know from the central theorem of space curves, that for given curvatures κ_i, $1 \leq i \leq n-1$ there exists a curve with these κ_i and any two such curves differ only by a translation followed by a rotation [element of SO(n)] [15], [16]. The curvatures therefore totally determine the shape of a space curve but do not tell anything about its position. This makes these parameters well suited as curve descriptors. The curvature κ_1 is a first order feature of a n-D curve.

Let $I \subseteq \mathbb{R}$ be an interval, then a C^1-mapping k: $I \to \mathbb{R}^n$ is called a *parameter curve* and $k(I)$ is called a *space curve.* Further, let $t \in I$ be the parameter of k then the *tangent* $dk/dt =: \dot{k}$ exists for all curves. The *arc length* $s(t)$ is $s(t) := \int_{t_0}^{t} \sqrt{\dot{k}^2}\, d\tilde{t}$. If $ds/dt = \sqrt{\dot{k}^2} \neq 0$, $\forall\, t$, i.e., k is a regular curve then $s \to t$ and $t \to s$ are valid parameter transformations. In the following, s will be the arc length and $'$ the derivative with respect to it. In this parameterization, we have the favorable properties $\|k'\| = 1$ and $k'k'' = 0$.

A *local* orthonormal basis $\{v_i\}$ can be constructed iteratively for a curve if $\dot{k}(t)$, $\ddot{k}(t)$, $\ldots$, $k^{(n-1)}(t)$ are linearly independent [15]. In this basis, the Frenet-equations can be formulated [16]. For a parameter curve k: $I \to \mathbb{R}^n$, unambiguous numbers $\kappa_1, \ldots, \kappa_{n-1}$ exist

$$\mathbf{K} = \begin{pmatrix} 0 & -\kappa_1 & 0 & \cdots & \cdots & 0 \\ \kappa_1 & 0 & -\kappa_2 & \cdots & \cdots & 0 \\ 0 & \kappa_2 & 0 & \cdots & \cdots & 0 \\ \vdots & \vdots & \vdots & \vdots & \vdots & \vdots \\ 0 & 0 & 0 & \cdots & 0 & -\kappa_{n-1} \\ 0 & 0 & 0 & \cdots & \kappa_{n-1} & 0 \end{pmatrix} \quad (1)$$

for which holds $V' = V\mathbf{K}$, where $V := (v_1, \ldots, v_n)$. Here, the κ_i is the ith *curvature* of the curve. From $v_1' = \kappa_1 v_2$, we see

immediately how to compute the curvature $\kappa_1 \equiv \kappa$ as $v_1 = k'$ and from the iterative construction of the basis $v_2 = k''/||k''||$ we obtain

$$\kappa = ||k''||. \tag{2}$$

From (2), we see that the curvature is always greater or equal to zero. Indeed for space curves it does not make sense to speak of a signed curvature in a coordinate independent description. In contrary to closed surfaces there is no border separating two distinct parts of space. By choosing an origin one can speak of signed curvature also for space curves.

Example: The circular helix, a parameterization is

$$k(t) = (r\cos t,\, r\sin t,\, ht), \qquad t \in \mathbb{R} \tag{3}$$

where h is the pitch, r the radius, and the helix is winding around the z-axis. With the parameterization of the curve and the arc length factor $ds/dt = \sqrt{r^2 + h^2}$, κ can be computed using the previous formulas

$$\kappa = \frac{r}{r^2 + h^2}. \tag{4}$$

II. Theory of Space Curves in Grey-Value Images

The local orthonormal basis $\{v_i\}$ can be obtained from the grey-level images itself by local orientation analysis.

A. Orientation Field: A Local Orthonormal Basis

In order to obtain the orientation field along a space curve embedded in a n-D image we use the gradient structure tensor (GST) [3], [9], [17]–[20]. For any image I, we can always compute the GST: $G_{ij} = \overline{I_i I_j}$, $1 \le i, j \le n$, where the lower index denotes a partial spatial derivative. The overhead bar denotes smoothing which is done per element of G, where each element is a n-D image. The GST can be expanded in terms of the eigenvalues λ_i and eigenvectors u_i as $G = \sum_i^n \lambda_i u_i u_i^t$, with $\lambda_1 \ge \lambda_2 \ge \cdots \ge \lambda_n$. The eigenvectors of the GST contain information about the local structure in the image. We can compute the largest λ_1 and smallest eigenvalue λ_n and the associated eigenvector for any dimension of the image by using the power method [21]. For the smallest eigenvalue, G has to be inverted, which becomes time consuming for large n. In the 2-D or 3-D case analytic solutions are possible and much faster [9], [19]. For line like structures the tangent orientation is given by the "smallest" eigenvector u_n. A normalized line detector is the ratio $(\lambda_{n-1} - \lambda_n)/(\lambda_{n-1} + \lambda_n)$ [9], [19].

All derivatives are implemented as convolutions with Gaussian derivatives. The scale σ_g denotes the resolution at which the Gaussian derivatives are computed. The size of the tensor smoothing σ_T defines how local the image structure is computed.

The local set of eigenvectors $\{u_i\}$ of the GST consists of the same set of vectors $\{v_i\}$ as the local orthonormal basis. The ordering, however, is different.

B. Discontinuity of the Orientation Field

Unfortunately the calculated orientation field u_n contains a discontinuity mod π [18], i.e., the direction of the line is undefined. Computation of partial spatial derivatives of the orientation field are not possible without some preparation. In general, a mapping to a higher dimensional space is needed to solve the discontinuity problem. For example, in 2-D, the phase jump can be resolved by doubling the angle of the gradient vector [1], [10].

C. Knutsson Mapping

Removing the phase jump in a n-D field is not a trivial task. Knutsson has introduced a mapping

$$M(x) = \frac{xx^t}{||x||} \tag{5}$$

that removes that discontinuity [18] while being distance preserving. The mapping satisfies the following three requirements: let $x \in \mathbb{R}^n$

- *uniqueness:* $M(x) = M(-x)$, this removes the phase jump;
- *uniformity:* $||\delta M(x)|| = \sqrt{2}||\delta x||$ for $||x|| = const$, locally preserves the angle metric;
- *polar separability:* $||M(x)|| = f(||x||)$, information carried by the magnitude of x normally does not depend on the angle.

For a comprehensive review on the problem of orientation representation, the connection between the Knutsson mapping, and the gradient structure tensor, see [22].

D. Curvature in n-D Grey-Value Images

Our goal is to compute the curvature via (2) $\kappa = ||k''||$. We start with the tangent orientation $v_n \equiv T \equiv k'$ obtained with the GST. Here, we already have the first derivative. The discontinuity problem (discussed previously) prevents direct computation of the derivative of T along v_n. This is solved by mapping the tangent orientation T via the quadratic mapping M to a continuous representation. The elements of $M(T)$ form a new n^2-D vector w. The ordering of the elements in this vector w does not influence our curvature estimation, because we only evaluate a norm, as shown in (8), which is independent of a permutation of the elements of w.

Now, we calculate the derivative of w in the direction of the tangent T [15], which is again a n^2-D vector

$$\frac{\partial w}{\partial T} = \mathbf{DM} \cdot T \tag{6}$$

where $\mathbf{DM}$ is the $n^2 \times n$ functional matrix

$$\mathbf{DM} = \begin{pmatrix} \frac{\partial w_1}{\partial x_1} & \frac{\partial w_1}{\partial x_2} & \cdots & \frac{\partial w_1}{\partial x_n} \\ \vdots & & & \vdots \\ \frac{\partial w_{n^2}}{\partial x^1} & \frac{\partial w_{n^2}}{\partial x_2} & \cdots & \frac{\partial w_{n^2}}{\partial x_n} \end{pmatrix}. \tag{7}$$

From the uniform stretch requirement of M we know how to scale the norm of a variation vector δx. Thus, starting from (2)

and the mapping $M(T)$ we obtain a new expression for the curvature

$$\kappa = \frac{1}{\sqrt{2}} \left\| \frac{\partial M(T)}{\partial T} \right\|. \tag{8}$$

We are aware of the fact that we cannot take it for granted that (8) represents the curvature of the original curve. First, we apply a nonlinear mapping M to the tangent orientation T and then in the mapped space linear operations, derivative and projection, are done. The reason why (8) is indeed another form of (2), is the uniform stretch requirement imposed on the mapping M, that ensures that there is a fixed relation between the norms of the mapped and the original vector.

E. Method in 2-D

Let us assume that the 2-D tangent orientation is given $T = \binom{f(x,y)}{g(x,y)}$,where f, g: $\mathbb{R}^2 \to \mathbb{R}$ are arbitrary functions. The mapped vector w is

$$w = \frac{1}{\sqrt{f^2+g^2}} \begin{pmatrix} f^2 \\ fg \\ gf \\ g^2 \end{pmatrix}. \tag{9}$$

Having the vector w explicitly, we construct the functional matrix, compute the projection onto the tangent direction (6) and then we can calculated the curvature using (8)

$$\kappa = \left| \frac{gf(\partial_x f) - f^2(\partial_x g) + g^2(\partial_y f) - fg(\partial_y g)}{f^2+g^2} \right|. \tag{10}$$

If we have the 2-D orientation field $\phi(x, y)$ given, then the tangent $T = \binom{-\sin\phi(x,y)}{\cos\phi(x,y)}$. Filling in this tangent in (10) and simplifying the expression with the help of the trigonometric relations, we get

$$\kappa = \left| \sin\phi \frac{\partial \phi}{\partial x} - \cos\phi \frac{\partial \phi}{\partial y} \right| = \left| \frac{\partial \phi}{\partial c} \right| \tag{11}$$

where c is the contour.

At this point, we are able to state that our method of calculating the curvature via the mapping in a higher dimensional space is consistent with the standard definition of curvature in 2-D. Also the isophote curvature formula in 2-D can be obtained by (10) with the gradient being $g = (I_x, I_y)$, the contour $c = (-I_y, I_x)$ and therefore the isophote tangent $T = c/\|c\| = (-I_y, I_x)/\sqrt{I_x^2 + I_y^2}$. The indices being partial derivatives. Filling in this tangent in (10), we get the isophote curvature formula [1], [7], [8]

$$\Rightarrow \kappa = \left| \frac{-(I_{xx}I_y^2 - 2I_xI_yI_{xy} + I_{yy}I_x^2)}{(I_x^2+I_y^2)^{3/2}} \right|. \tag{12}$$

III. Evaluation of the Algorithm

To assess the performance of the proposed estimator we will apply it to synthetic test images of various scales and hampered by noise.

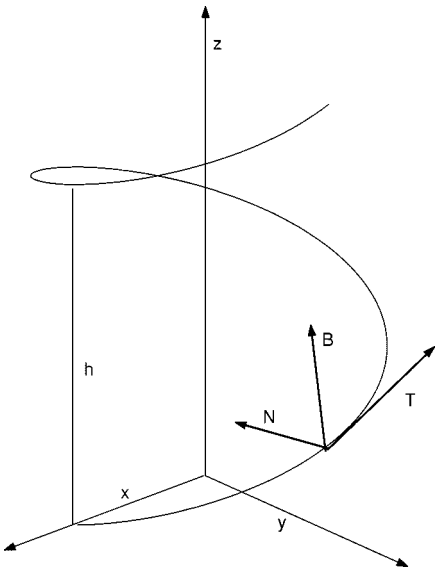

Fig. 1. Center line of a grey-level helix.

A. Test Images

Definition: Under a space curve in a grey-value image, we understand a line of constant grey-value, i.e., an isophote (level-set). It should be noted that such isophotes are implicitly represented by the voxel-values of a properly sampled bandlimited image.

To evaluate the algorithm on space curves, some proper test images are needed that reflect this definition.

A general method of creating smooth and approximately bandlimited space-curves in images is described in the following. One has to consider that a suitable test image must be bandlimited before sampling, otherwise one might encounter problems due to aliasing [8]. We do this by computing the distance from every voxel in the image to the mathematical function and assign it to the voxel. In the next step, the image is multiplied by itself to create a steeper slope; subsequently, an erfclip operation [23] is applied to produce a smooth space-curve, embedded in an image.

In 2-D, we use a simple ring as a test image. In 3-D, as a first step we create a torus of arbitrarily orientation. In a second step we study the simplest possible test object in 3-D not only having curvature. The object with constant curvature and torsion is the circular helix (3). So we finally get a smooth representation of a torus/helix which looks like a string spaghetti shaped into a torus/helix. This guarantees a sub-pixel precision and approximately bandwidth limitation. The image consists of an isophote (same grey level) center line and isocylinders around it.

In Fig. 1, the center line of a grey-level helix is shown, where the line indicates constant grey-value. The vectors given in the figure represent the local orthonormal basis (Section I-A), $T \equiv v_1$ being the tangent, $N \equiv v_2$ the normal and $B \equiv v_3$ the binormal vector. In Fig. 2, an isosurface plot of the smooth string shaped into a spaghetti is shown. The isocap through the spaghetti shows the isocylinder around the imaginary center line. In Fig. 3, a cross section through a test object is shown, you can clearly see the Gaussian profile with the top being the centerline.

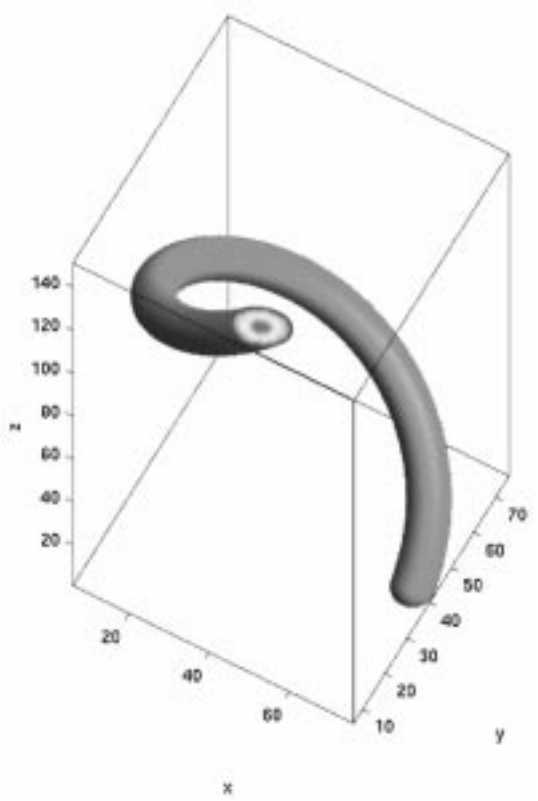

Fig. 2. Isosurface plot of a grey-level helix.

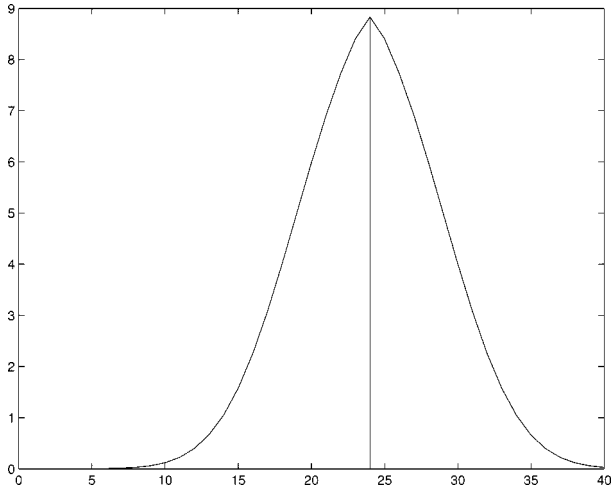

Fig. 3. Cross section through a test object.

B. Ring

To start off in 2-D, we generate smooth rings with different radii and signal strength $S = 1$. To measure the robustness of the estimator we add different levels of Gaussian noise. We use the definition SNR$= 20\log(S/\sigma_n)$, where σ_n^2 is the variance of the Gaussian noise. The results are depicted in Fig. 4. The different noise levels are always calculated at the same radii, but slightly shifted in the figure for a better display. The error bars indicate the standard deviation over 40 runs. A tensor smoothing $\sigma_T = 5$ and a gradient smoothing $\sigma_g = 1$ was used. For SNR $= 10$ dB

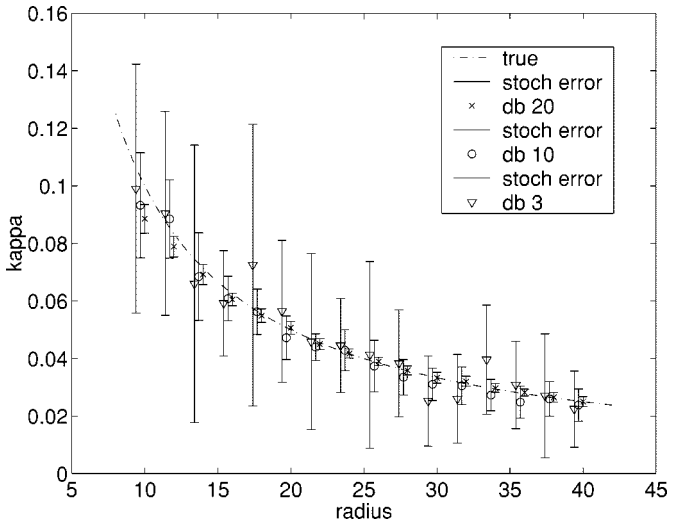

Fig. 4. Average curvature estimation on a 2-D ring for different noise levels.

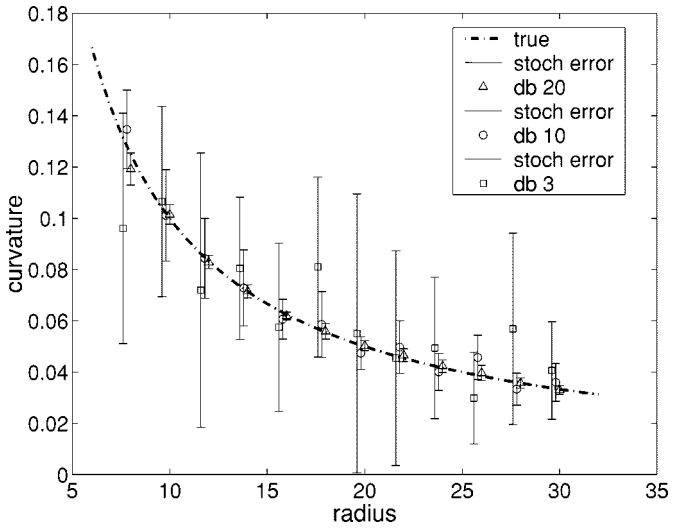

Fig. 5. Average curvature estimation on a torus for different noise levels.

the average relative error is smaller than 10%. The estimator is unbiased.

C. Torus

The torus image has a grey-value range from zero to one; therefore, SNR $= -20\log\sigma_n$. Again, we use $\sigma_T = 5$ and $\sigma_g = 1$. The performance of the estimator is tested over 20 runs for different noise levels (see Fig. 5). The error bars indicate the standard deviation. The different noise levels are again shifted in the figure for better display. The error bars include even for the high noise level (3 dB) the true value.

D. Helix

The curvature $\kappa = r/(r^2 + h^2)$ (4) of the helix depends on the two parameters r and h which scale the helix. For increasing size of the helix radius the curvature first rises, being at its maximum at $r = h$ and then decreasing (Fig. 12). In order to make a scale invariant statement about the performance of our algorithm we sample the scale space r, h, generate the according test

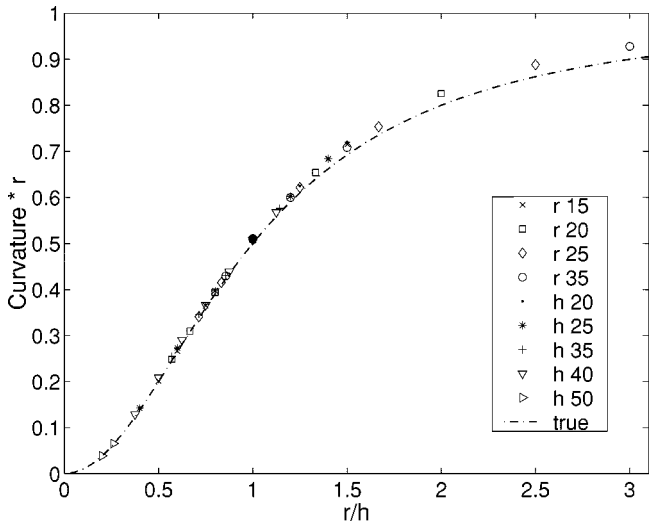

Fig. 6. Curvature of the helix, scale invariant.

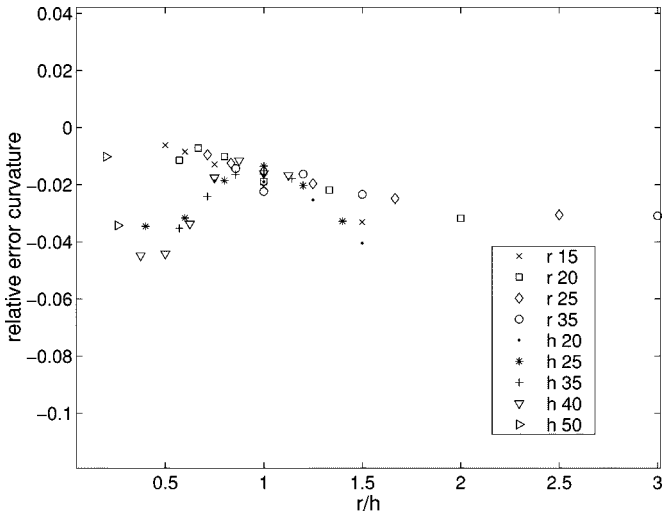

Fig. 7. Relative error, scale invariant.

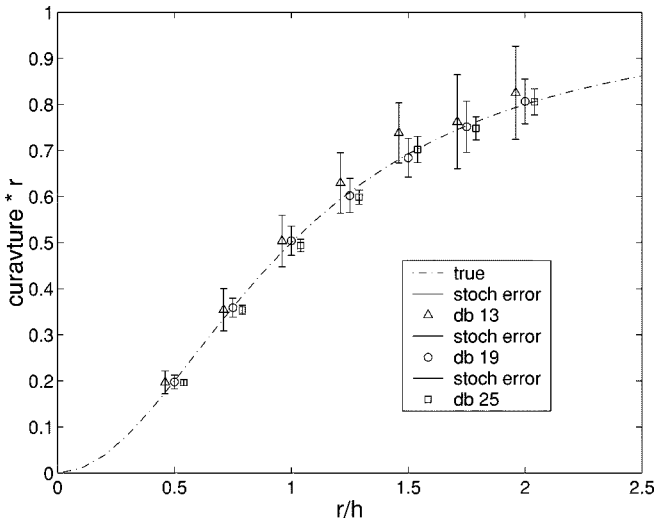

Fig. 8. Curvature estimation with added noise.

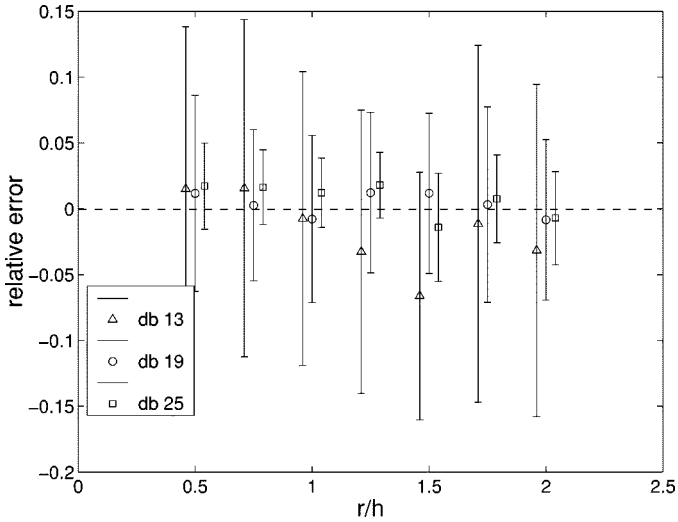

Fig. 9. Relative error in curvature estimation with added noise.

images and compute the curvature of the center line. Therefore, we rewrite (4) to

$$\kappa = \frac{\frac{r}{h^2}}{1+\frac{r^2}{h^2}} \quad \text{and} \quad \kappa r = \frac{x^2}{1+x^2}, \quad x = \frac{r}{h}. \tag{13}$$

Now, we deal with dimensionless quantities x and κr, which are suitable to show that our estimation works fine over a wide range of scales. In Fig. 6, we plot the theoretical prediction and our calculations, in which the different symbols indicate helices having either the same radius or pitch. Because our estimation stays so close to the true value over a wide range of scales, we conclude that for all values in between our sampled grid points the estimation works as well. The relative error of the estimation shown in Fig. 7 is smaller than 5% over a range from $r/h \in [0.1, 3.0]$.

1) Influence of Noise:

- *Noise for different helix scales*

  In the same scale invariant manner as for Fig. 6, we investigate the performance under noisy circumstances. In Fig. 8, the results are shown for 13, 19, and 25 dB, where the error bars indicate the standard deviation for 20 runs. The estimation is unbiased, since the error bars always intersect the true curvature. The relative error is shown in Fig. 9.

- *Studies along a cross section of the helix profile*

  For one helix ($r = 10$, $h = 20$), we add noise (SNR $= 19$ dB) to the image and plot the computed curvature (mean over 20 runs) and the standard deviation in Fig. 10 along a cross section of the helix (see Fig. 3). Again we see that the mean remains around the true value, and the variation stays approximately constant. It should be pointed out that we see here not only the isophote line at the point where the mathematical helix would lie but a cross section through the 15 pixel diameter of the helix. Due to the regularization effect of the GST, we can estimate the true curvature even if we are not at the exact position. If we choose a small tensor smoothing σ_T, then the relative error at the exact point becomes smaller but for the surrounding values it becomes larger.

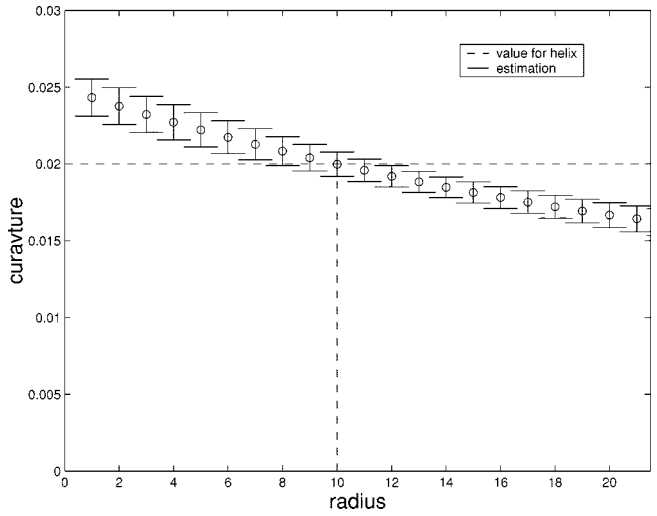

Fig. 10. Curvature along a cross section, 19 dB.

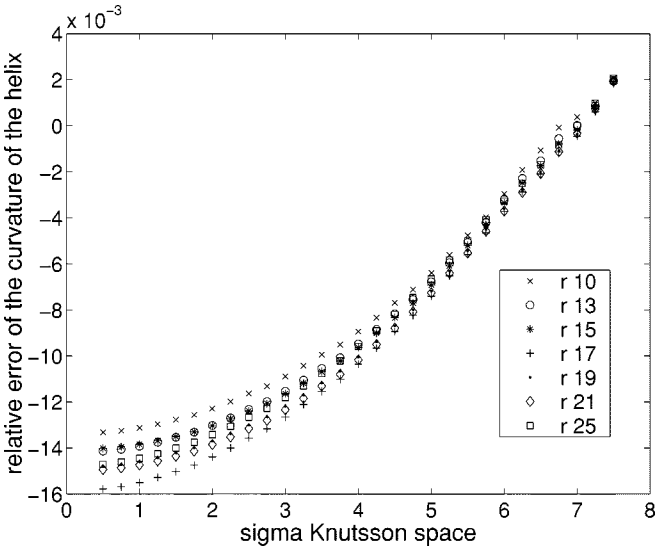

Fig. 11. Influence of σ_K.

2) Influence of the Gaussian Derivative in the Mapped Space: For a limited number of helices ($h = 50$, $r = 10$–25), we investigate the dependency of the relative error of the curvature on σ_K, the standard deviation of the Gaussian derivative in the mapped space (6) (compare Fig. 11). Here, we observe an overall σ_K^2 dependency in the relative error.

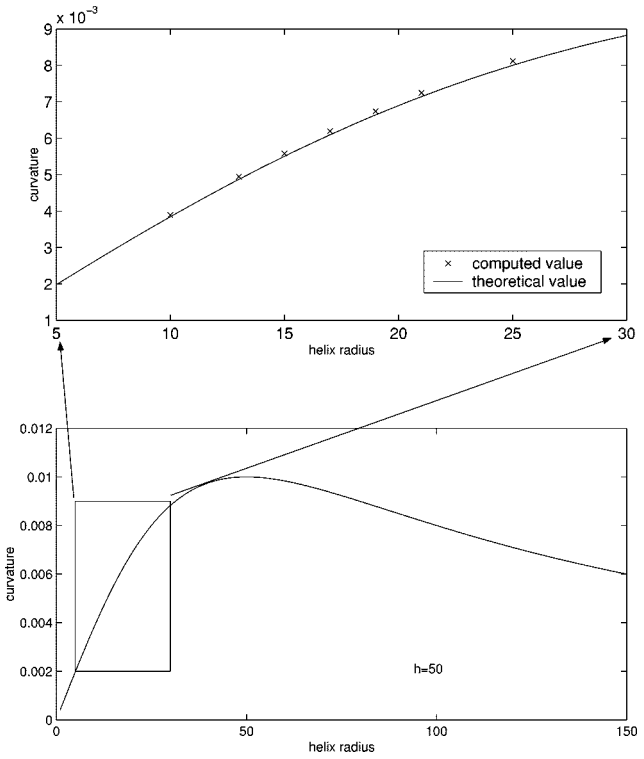

Fig. 12. Change with the radius.

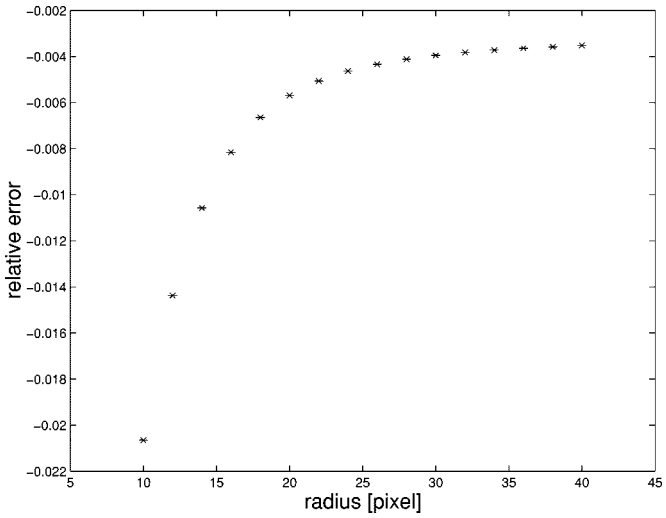

Fig. 13. Relative error for curvature estimation of a 2-D ring.

IV. Comparison With a Segmentation Based Approach

Coeurjolly *et al.* [14] presented a purely discrete algorithm to compute curvature in images based on discrete osculating circles as an extension to the method classification done by Worring and Smeulders [4].

The estimation error of Coeurjolly *et al.* is dependent on the resolution of the grid. Our algorithm is independent of this quantity as long as the object is not undersampled. Their estimation error on a 2-D noise free disk is about 2.5% for a circle with radius 50 and about 1% for a circle with radius 100 pixels (corresponding to grid step size of 1/50 and 1/100 resp.). On noise free 2-D rings, our method performs with a relative error of about 0.5% for radii greater than 25 pixels (see Fig. 13). For smaller radii, the estimation is less reliable due to the influence of opposing ring edges in the smoothing of the gradient structure tensor elements for $\sigma_T = 5$, but still more accurate than the discrete approach. In the case of noisy images, the segmentation algorithm plays a key role for the quality of the curvature estimation; this is not the case for our proposed method.

Measuring the curvature along the boundary of a circle (40 pixel radius) they get a relative error of about $\pm 15\%$ due to quantization. Our method gives only a relative error of $\pm 1.2\%$ (compare Fig. 14).

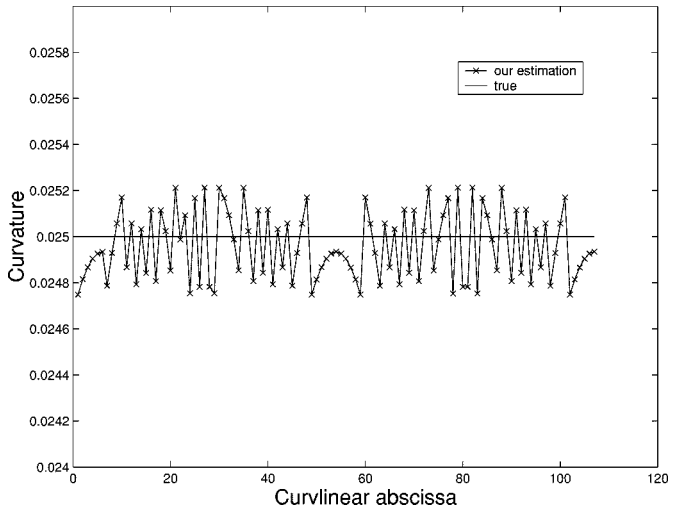

Fig. 14. Curvature along a circle contour.

V. Applications

In fluorescent confocal microscopy, especially in biological life time applications, 3-D time series are acquired [24], [25]. Typically, these images contain moving bright spots. Here, it could be of interest to compute the acceleration of the spots. The acceleration is related to the curvature of the spatiotemporal space curve formed by the moving spots. The acceleration a can be computed from the 4-D image with the notation as in Section I-A as follows [26]:

$$\left(\frac{ds}{dt}\right)^2 = ||\dot{k}||^2 = |v|^2 \tag{14}$$

$$a = |\dot{v}|T + |v|^2\kappa(s)N. \tag{15}$$

This is the classical expression of the tangential and the normal components of the acceleration.

The velocity v can be computed by, e.g., optical flow [24], [17] or via the gradient structure tensor. In a spatiotemporal 4-D image (x, y, z, t), the orientation of the space curve, formed by a moving spot, is a measure for the velocity of the spot [27], [28]. It should be noted that the eigenvalue analysis of the gradient structure tensor which is used to measure the 4-D orientation does not give direction information. We can, however, retrieve the velocity vector if we shift the discontinuity of the orientation field to the time dimension. This is reasonable as we know there is a causal connection between the time frames, i.e., $\Delta u_t > 0$. We can retrieve the components of the velocity vector as follows:

$$v_i = \frac{\partial u_i}{\partial t} \approx \frac{\Delta u_i}{\Delta u_t} \qquad 1 \le i \le 3 \tag{16}$$

where u_i are the eigenvectors of the gradient structure tensor.

VI. Conclusion

We have shown that the curvature of space curves embedded in n-D grey-value images can be estimated using the formulas given by differential geometry adjusted to the higher dimensional space mapped by the Knutsson mapping. Our new estimation formula (8) reduces in 2-D to the known expression, which clearly indicates that our work is consistent with older work. Furthermore, the estimation is unbiased, which even holds in the presence of noise. The curvature calculation is clearly independent of the scale of the objects as shown by our computations. Our grey-value based approach is clearly superior to a discrete curvature estimation.

Acknowledgment

The calculations were performed with the MATLAB toolbox DIPimage [29].

References

[1] M. van Ginkel, J. van de Weijer, P. W. Verbeek, and L. J. van Vliet, "Curvature estimation from orientation fields," in *Proc. 11th Scandinavian Conf. Image Analysis*, B. K. Ersboll and P. Johansen, Eds. Kangerlussuaq, Greenland, June 7–11, 1999, pp. 545–551.

[2] K. Nordberg, H. Knutsson, and G. Granlund, "Signal representation using operators," Linköping Univ., Linköping, Sweden, Tech. Rep. LiTH-ISY-I-1342, 1992.

[3] B. Jähne, *Digital Image Processing*, 4th ed. New York: Springer, 1997.

[4] M. Worring and A. W. M. Smeulders, "Digital curvature estimation," *CVGIP: Image Understand.*, vol. 58, no. 3, pp. 336–382, 1993.

[5] ——, "The accuracy and precision of curvature estimation methods," in *Proc. 11th IAPR Int. Conf. Pattern Recognition*, The Hague, The Netherlands, 1992, pp. 139–142.

[6] P. W. Verbeek, "A class of sampling-error free measures in oversampled band-limited images," *Pattern Recognit. Lett.*, vol. 3, pp. 287–292, 1985.

[7] P. Breton and S. W. Zucker, "Shadows and shading flow fields," in *Proc. IEEE Conf. Computer Vision and Pattern Recognition*, San Francisco, CA, 1996, pp. 782–789.

[8] L. J. van Vliet and P. W. Verbeek, "Curvature and bending energy in digitized 2D and 3D images," in *Proc. 8th Scandinavian Conf. Image Analysis*, Tromsø, Norway, 1993, pp. 1403–1410.

[9] J. van de Weijer, L. J. van Vliet, P. W. Verbeek, and M. van Ginkel, "Curvature estimation in oriented patterns using curvilinear models applied to gradient vector fields," *IEEE Trans. Pattern Anal. Machine Intell.*, vol. 23, pp. 1035–1042, Sept. 2001.

[10] H. Knutsson, "Producing a continuous and distance preserving 5-D vector representation of 3-D orientation," in *IEEE Comput. Soc. Workshop on Computer Architecture for Pattern Analysis and Image Database Management*, Miami Beach, FL, Nov. 18–20, 1985, pp. 175–182.

[11] M. Boutin, "Numerically invariant signature curves," *Int. J. Comput. Vis.*, vol. 40, no. 3, pp. 235–248, 2000.

[12] N. Kehtarnavaz and R. J. P. de Figueiredo, "A 3-d contour segmentation scheme based on curvature and torsion," *IEEE Trans. Pattern Anal. Machine Intell.*, vol. 10, no. 5, pp. 707–713, 1988.

[13] K. V. Mardia, R. J. Morris, A. N. Walder, and J. J. Koenderink, "Estimation of torsion," *J. Appl. Statist.*, vol. 26, pp. 373–381, 1999.

[14] D. Coeurjolly, S. Miguet, and L. Tougne, "Discrete curvature based on osculating circle estimation," in *Visual Form 2001, 4th Int. Workshop on the Visual Form*, C. Arcelli, L. P. Cordella, and G. Sanniti fi Baja, Eds. New York: Springer, May 2001, vol. 2059, pp. 303–312.

[15] I. N. Bronstein, K. A. Semendjajew, G. Musiol, and H. Mühlig, *Taschenbuch der Mathematik*, 4th ed. Frankfurt, Germany: Verlag Harri Deutsch, 1999.

[16] M. Spivak, *A Comprehensive Introduction to Differential Geometry*. Berkeley, CA: Publish or Perish, 1979, vol. 2.

[17] M. Kass and A. Witkin, "Analyzing oriented patterns," *Comput. Vis. Graph. Image Process.*, vol. 37, pp. 362–385, 1987.

[18] H. Knutsson, "Representing local structure using tensors," in *Proc. 6th Scandinavian Conf. Image Analysis*, Oulu, Finland, June 19–22, 1989, pp. 244–251.

[19] G. M. P. van Kempen, N. van den Brink, L. J. van Vliet, M. van Ginkel, and P. W. Verbeek, "The application of a local dimensionality estimator to the analysis of 3D microscopic network structures," in *SCIA'99, Proc. 11th Scandinavian Conf. Image Analysis*, Kangerlussuaq, Greenland, June 7–11, 1999, pp. 447–455.

[20] S. di Zeno, "A note on the gradient of a multi-image," *Comput. Vis., Graph., Image Process.*, vol. 33, pp. 166–125, 1986.

[21] G. H. Golub and C. F. van Loan, *Matrix Computations*, 3 ed. Baltimore, MD: John Hopkins Univ. Press, 1996.

[22] *A systematic approach to nD orientation representation*, submitted for publication.
[23] L. J. van Vliet and P. W. Verbeek, "Better geometric measurements based on photometric information," in *Proc. IEEE Instrumentation and Measurement Technol. Conf., IMTC94*, 1994, pp. 1357–1360.
[24] C. B. J. Bergsma, G. J. Streekstra, A. W. M. Smeulders, and E. M. M. Manders, "Velocity estimation of spots in 3d confocal images sequences of living cells," *Cytometry*, vol. 43, no. 4, pp. 261–272, 2001.
[25] E. M. M. Manders, A. E. Visser, A. Koppen, W. C. de Leeuw, R. van Liere, G. J. Brakenhoff, and R. van Driel, "Chromatin dynamics during the formation of the interphase nucleus," *J. Cell Sci.*, to be published.
[26] T. Frankel, *The Geometry of Physics*. Cambridge, U.K.: Cambridge Univ. Press, 1997.
[27] J. Karlholm, "Local signal models for image sequence analysis," Ph.D. dissertation, Linköping Univ., Linköping, Sweden, 1998.
[28] B. Jähne, *Spatio–Temporal Image Processing*. Berlin, Germany: Springer-Verlag, 1993, vol. 751 in Lecture Notes in Computer Science.
[29] C. L. Luengo Hendriks, L. J. van Vliet, B. Rieger, and M. van Ginkel. (1999) DIPimage: A scientific image processing toolbox for MATLAB. Pattern Recognit. Group, Dept. Appl. Phys., Delft Univ. Technology, Delft, The Netherlands. [Online]. Available: http://www.ph.tn.tudelft.nl/DIPlib.

Bernd Rieger received the M.Sc. degree in physics from the Munich University of Technology, Munich, Germany, in 1999. He is currently pursuing the Ph.D. degree in image processing and analysis at Delft University of Technology, Delft, The Netherlands.

His research interests include motion estimation for 3-D image sequences and development of grey-value based estimators for analysis of structure in images.

Lucas J. van Vliet was born in 1965. He received the M.Sc. degree in applied physics in 1988 and the Ph.D. degree (cum laude) in 1993. His dissertation entitled "Grey-scale measurements in multi-dimensional digitized images" presents novel methods for sampling-error free measurements of geometric object features.

He is a Full Professor in multidimensional data analysis with the Faculty of Applied Sciences, Delft University of Technology, Delft, The Netherlands. He has worked on various sensor, restoration, and measurement problems in quantitative microscopy. His current research interests include segmentation and analysis of objects, textures, and structures in multidimensional digitized images from a variety of imaging modalities.

Dr. van Vliet was awarded a fellowship from the Royal Netherlands Academy of Arts and Sciences (KNAW) in 1996.